Article

pubs.acs.org/Biomac

Light-Responsive Micelles of Spiropyran Initiated Hyperbranched Polyglycerol for Smart Drug Delivery

Suhyun Son, Eeseul Shin, and Byeong-Su Kim*

Department of Chemistry and Interdisciplinary School of Green Energy, Ulsan National Institute of Science and Technology (UNIST), Ulsan 689-798, Korea

Supporting Information

ABSTRACT: Light-responsive polymeric micelles have emerged as site-specific and time-controlled systems for advanced drug delivery. Spiropyran (SP), a well-known photochromic molecule, was used to initiate the ring-opening multibranching polymerization of glycidol to afford a series of hyperbranched polyglycerols (SP-*hb*-PG). The micelle assembly and disassembly were induced by an external light source owing to the reversible photoisomerization of hydrophobic SP to hydrophilic merocyanine (MC). Transmission electron microscopy, atomic force microscopy, UV/vis spectroscopy, and dynamic light scattering demonstrated the successful assembly and disassembly of SP-*hb*-PG micelles. In addition, the critical micelle concentration (CMC) was determined through the fluorescence analysis of pyrene to confirm the amphiphilicity of respective SP-*hb*-PG$_n$ (n = 15, 29, and 36) micelles, with CMC values ranging from 13 to 20 mg/L, which is correlated to the length of the polar polyglycerol backbone. Moreover, the superior biocompatibility of the prepared SP-*hb*-PG was evaluated using WI-38 cells and HeLa cells, suggesting the prospective applicability of the micelles in smart drug delivery systems.

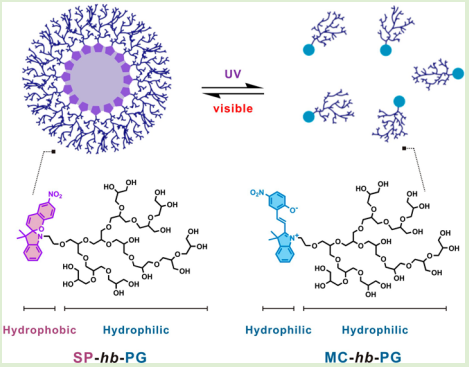

INTRODUCTION

Over the past few decades, drug delivery systems have advanced to achieve time-controlled and site-specific delivery of therapeutic agents to enhance the efficacy of drugs while minimizing undesirable side effects.[1,2] Self-assembled nanostructures have long been exploited as potential drug delivery carriers, including liposome, dendrimer, micelle, and artificial DNA.[3,4] In particular, self-assembled polymeric micelles have been highlighted as promising vehicles based on their distinctive features, such as high loading capacity, and enhanced solubility and circulation lifetime of active therapeutics, as well as prioritized accumulation at tumor sites owing to the enhanced permeability and retention (EPR) effect.[5−7] More importantly, the high tunability of their chemical and physical properties based on the choice of monomer, polymerization degree, architecture, and other parameters, makes self-assembled polymeric micelles among the top choices as prospective carriers.[8]

Despite the advantages of self-assembled polymeric micelles, the sophisticated delivery of active therapeutics in a time-specific and stimuli-specific manner continues to be a challenging endeavor. To meet this objective, smart drug delivery carriers that encapsulate drugs and release them at a targeted region in response to external stimuli such as pH, light, redox, temperature, and biological stimuli have been actively studied.[9−11] For example, Zhao and co-workers have extensively investigated the development of light-responsive micelle systems owing to the feasibility of remote triggering of active therapeutic release and high controllability over the drug release profile using a specific wavelength of light. Along the same line, various light-responsive smart delivery systems have been reported to date that operate on the principle of photoisomerization, photoinduced cleavage of the photochromic moiety or junction, and reversible photo-cross-linking.[12−15]

As an alternative to traditional poly(ethylene glycol) (PEG), which is the most biocompatible synthetic polymer, its polyether analogue, hyperbranched polyglycerol (*hb*-PG), is actively investigated, owing to its excellent biocompatibility and advantages over PEG, such as the ease of synthesis, controllable structure, multi (or hetero)-functional groups, and oxidation stability.[16−19] The recent synthetic advancement by the Frey group has allowed the development of well-defined and complex architectures of polyglycerols with relatively low polydispersity.[17,20] These polyglycerols also exhibit flexibility of the physicochemical properties by the protected monomer, variation of initiators, and combination with other polymerization techniques.[21−23] Recently, polyglycerols with varying architectures have been designed and synthesized for biomedical applications. Brooks and co-workers have studied the suitability of hydrophobically functionalized hyperbranched polyglycerols for use as synthetic albumin substitutes and

Received: November 11, 2013
Revised: January 15, 2014
Published: January 16, 2014

Scheme 1. Illustration of Light-Responsive Micelle Assembly and Disassembly of Spiropyran-Hyperbranched-Polyglycerol (SP-*hb*-PG)[a]

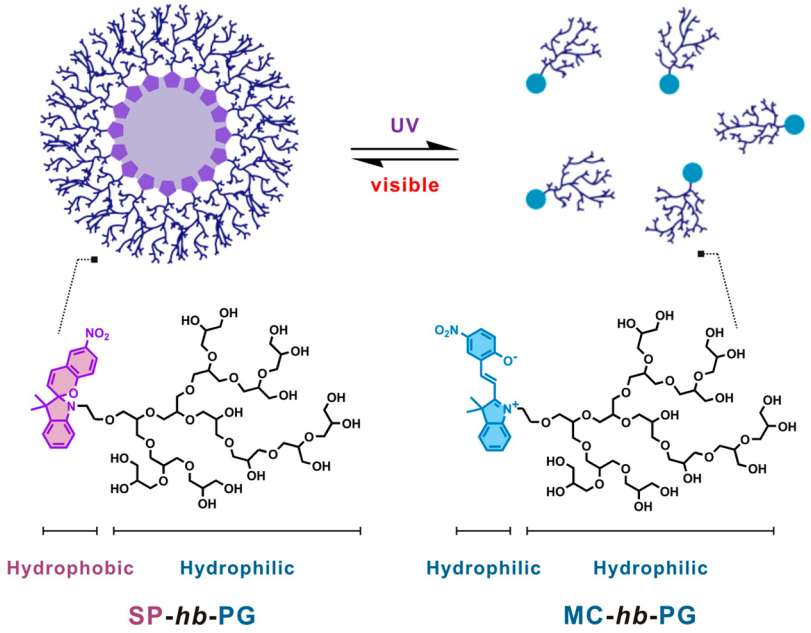

[a]Micelle structure is not drawn to scale.

general drug delivery vehicles.[24] In addition, our group has recently employed various architectures of the *hb*-PG in pH-responsive smart drug delivery systems.[25,26] However, there is no report in which the *hb*-PG is utilized in light-responsive drug delivery systems.

In this article, we present the design of photoresponsive micelles using spiropyran (SP) initiated hyperbranched polyglycerols (SP-*hb*-PG) and investigation of their potential in light-controlled release of model therapeutics (Scheme 1). Among the class of synthetic photoresponsive molecules, SP, a well-known photochromic molecule, was employed owing to its unique tunability, stability, and fast response time.[27] Specifically, SP can undergo a reversible transformation from colorless to pink-colored merocyanine (MC) upon UV irradiation with a marked increase in the polarity associated with the structural conversion from neutral to charge-separated zwitterions.[28] This solubility switching of SP from hydrophobic to hydrophilic can induce the destabilization of polymeric micelles of SP-*hb*-PG into individual chains (Scheme 1). Moreover, this destabilization induces controlled release of model hydrophobic therapeutics by UV irradiation.

EXPERIMENTAL SECTION

Materials. All reagents and solvents were purchased from Sigma Aldrich and Acros unless otherwise stated. Dry solvents purchased from Sigma-Aldrich were stored over molecular sieves. Deuterated DMSO-d_6 was purchased from Cambridge Isotope Laboratory, dried, and stored over molecular sieves.

Measurements. ^{1}H NMR spectra were acquired using a 400-MR DD2 spectrometer operating at 400 MHz, using DMSO-d_6 as a solvent. Gel permeation chromatography (GPC) was performed on a Tosoh HLC-8120 GPC equipped with a consecutive polystyrene gel column (TSK-GEL GMHHR-M and GMHHR-N) at 40 °C, using *N*-methylpyrrolidone containing 0.01 mol/L lithium bromide as an eluent at a flow rate of 1.0 mL/min; standard polystyrene samples were used for calibration in order to measure the number- and weight-averaged molecular weight (M_n and M_w). Matrix-assisted laser desorption and ionization time-of-flight mass spectrometry (MALDI-ToF) measurements were carried out on an Ultraflex III MALDI mass spectrometer. The laser system consisted of a pulsed UV laser, an attenuator that allowed the fine adjustment of the laser fluence, a lens system to focus the laser beam, and a mirror system to direct the beam into the ion source on the target plate. The standard was a N_2 laser with 337 nm wavelength (pulse energy of 150 μJ) and 3 ns pulse width for use with matrix components absorbing light of this wavelength (IVB product). α-Cyano-4-hydroxycinnamic acid (CHCA) was used as a matrix. A 10 g/L solution of the polymer in methanol and a 10 g/L solution of the matrix solution were prepared separately. The two solutions were then mixed and a 1 μL aliquot of the mixture was applied to a target plate, and the solvent was evaporated. The morphology of the SP-*hb*-PG micelle was investigated using transmission electron microscopy (TEM, JEM-2100, JEOL, Japan) and atomic force microscopy (AFM, Dimension 3100, Veeco, U.S.A.). Size distribution analysis of the SP-*hb*-PG micelles was performed using dynamic light scattering (DLS, BI-APD, Brookhaven Instrument, New York, U.S.A.). UV/vis spectrophotometer (UV-2550, Shimadzu) was used to measure absorbance of SP-*hb*-PG. UV irradiation was conducted using a UV lamp (B-100AP high-intensity UV lamp, 100 W).

Synthesis of a Spiropyran Derivative. 2-(3′,3′-Dimethyl-6-nitro-3′*H*-spiro[chromene-2,2′-indol]-1′-yl)-ethanol (spiropyran) was prepared according to the method reported in the literature.[29]

Polymerization of SP-*hb*-PG. SP (1 mmol) and cesium hydroxide monohydrate (0.8 mmol, 0.8 equiv) were placed in a Schlenk flask, benzene (20 wt %) was added, and the mixture was stirred for 2 h at 60 °C under a nitrogen atmosphere to produce cesium alkoxide. The initiator was dried in a vacuum oven for 2 h at 90 °C. After the initiator became powdery, dry diglyme (ca. 20 wt %) was added under a nitrogen atmosphere. Glycidol (30 mmol) diluted with dry diglyme (20 wt %) was then added over 12 h at 90 °C using a syringe pump. The reaction was terminated by addition of excess methanol and acidic cation exchange resin. After dissolving the polymer in methanol, the homogeneous polymer solution was precipitated and filtered into excess cold diethyl ether. The resulting material was dried under vacuum at 60 °C for 2 days.

Preparation of SP-*hb*-PG Micelle. A 1.0 mg sample of SP-*hb*-PG was dissolved in 1 mL of DMF, after which 4 mL of water was added dropwise over 1 h via a syringe pump to form micelles. Subsequently,

dx.doi.org/10.1021/bm401670t | *Biomacromolecules* 2014, 15, 628−634

Scheme 2. Synthetic Approach for Preparation of (a) Spiropyran Derivative Containing Hydroxyl Group and (b) SP-*hb*-PG Polymers

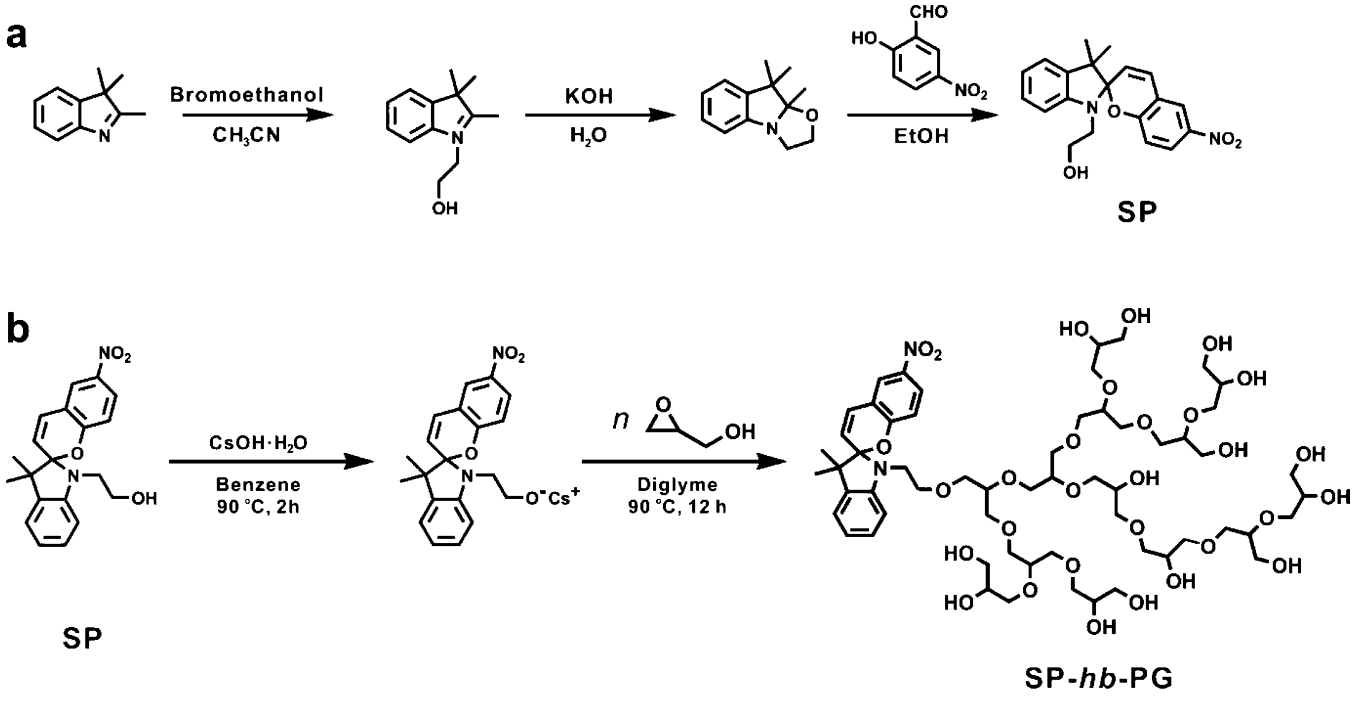

the polymer solution was dialyzed against DI water for 2 days to exchange the residual DMF. The solution was then filtered through a 0.22 μm syringe filter before DLS, TEM, and AFM analysis.

Pyrene Fluorescence Measurement and CMC Study. A total of 1.0 mg SP-*hb*-PG polymer was dissolved in 1.0 mL of DMF. A 10 μL solution of pyrene (5.2 mg/L in DMF) was added to the SP-*hb*-PG solution and the mixture was stirred for 30 min at room temperature. A total of 5 mL of DI water was then added to the solution at a rate of 0.5 mL/min using a syringe pump. The fluorescence of each pyrene-containing polymer micelle solution (with different concentrations) was measured at an emission wavelength of 372 nm using a fluorometer. The critical micelle concentration (CMC) values were determined by calculating the ratio of the fluorescence intensities at wavelengths of 339.06 and 332.04 nm.

Cytotoxicity Assay. Human epithelial carcinoma cells (HeLa) and human diploid cells (WI-38) were purchased from the Korean Cell Line Bank (Seoul, Korea). Cytotoxicity assay was performed using the traditional MTT assay. Cells were seeded in 96-well plates at a density of 1×10^4 cells per well and incubated for 24 h in 5% CO_2 at 37 °C. HeLa cells were cultured with Dulbecco's Modified Eagle's Medium, (DMEM, Life Technologies) with 10% fetal bovine serum (FBS) and 1% penicillin-streptomycin. WI-38 cells were incubated in Roswell Park Memorial Institute (RPMI) 1640 media (Life Technologies) with 10% FBS, 25 mM sodium bicarbonate, and 1% penicillin-streptomycin. After removing the culture medium, the wells were washed with PBS. Each well was then refilled with 90 μL of fresh Dulbecco's Modified Eagle's Medium (DMEM) and 10 μL of SP-*hb*-PG_n polymeric micelle solution. After an additional 24 h of incubation, thiazolyl blue tetrazolium bromide (MTT, Sigma-Aldrich) was added to each well of the cells (final conc. 0.5 mg/mL) and incubation was performed for 4 h. A solution of 100 μL of DMSO was replaced with SP-*hb*-PG solution to solubilize the MTT-formazan product, and the sample was incubated for a further 15 min at room temperature. The absorbance of the solution was read at a wavelength of 540 nm.

RESULTS AND DISCUSSION

Synthesis and Characterization of Spiropyran Initiated Hyperbranched Polyglycerol. SP was initially prepared according to a method described in the literature (Figure 2a).[29] The prepared SP exhibited a clear color transition from colorless to pink upon excitation with UV light at 365 nm, displaying the desired UV-responsive character. The amphiphilic polymer SP-*hb*-PG was synthesized via anionic ring-opening polymerization using the SP initiator generated by treatment with cesium alkoxide, followed by the slow addition of a glycidol monomer (Scheme 2b). Three different hyperbranched SP-*hb*-PG polymers varying in terms of the molecular weight of the *hb*-PG segment, which ranged from 1500 to 3000, were successfully prepared (Table 1). Initially,

Table 1. Characterization of Spiropyran Initiated Hyperbranched Polyglycerol

		M_n (g/mol)					
no.	composition	calcd	NMR[a]	GPC[b]	M_w/M_n[b]	DB[c]	CMC (mg/L)
1	SP-*hb*-PG_{15}	1500	2210	1690	1.77	0.53	13
2	SP-*hb*-PG_{29}	2500	2600	3100	1.79	0.54	19
3	SP-*hb*-PG_{36}	3000	2930	3870	1.92	0.53	20

[a]M_n determined via ^{1}H NMR spectroscopy. [b]M_n and M_w measured using GPC-RI in NMP with polystyrene standard. [c]Degree of branching (DB) is determined from inverse gated ^{13}C NMR spectroscopy and calculated according to Frey's equation (DB = $2D/2D + L$; see Supporting Information for details).

the molecular weight was determined from ^{1}H NMR by integrating the signals of the aromatic groups of the SP initiator at 8.3 ppm and those of the polyether backbone of *hb*-PGs in the range of 3.3 to 4.0 ppm (see Supporting Information, Figure S1). These values were consistent with the theoretical target molecular weights, as shown in Table 1. In addition, the M_n and the polydispersity index (M_w/M_n) of the prepared SP-*hb*-PG_n samples were determined via GPC-RI, which showed a relatively monomodal molecular weight distribution with reasonable PDI values for all hyperbranched polymers. Notably,

dx.doi.org/10.1021/bm401670t | Biomacromolecules 2014, 15, 628−634

the discrepancy between the M_n values from GPC and NMR became slightly higher as the molecular weight of the polymer increased, which could be attributed to the use of a linear polystyrene standard in measuring the molecular weight of the *hb*-PG.

Moreover, the hyperbranched nature of the SP-*hb*-PG was further confirmed by measuring the degree of branching (DB) via ^{13}C NMR and calculation using Frey's equation (DB = 2*D*/L13 + L14 + 2*D*; L13:1,3 linear portion, L14:1,4 linear portion, and D: dendritic portion; see Supporting Information, Figure S2). This equation indicates the ratio of the branched dendritic segment within the PG backbones that are composed of both linear and branched segments. The DBs of all polymers were determined to be about 0.53, which is in good agreement with that of other hyperbranched systems.[17]

The presence of each segment of SP and polyglycerol was also identified from the MALDI-ToF spectrum (Figure 1). As

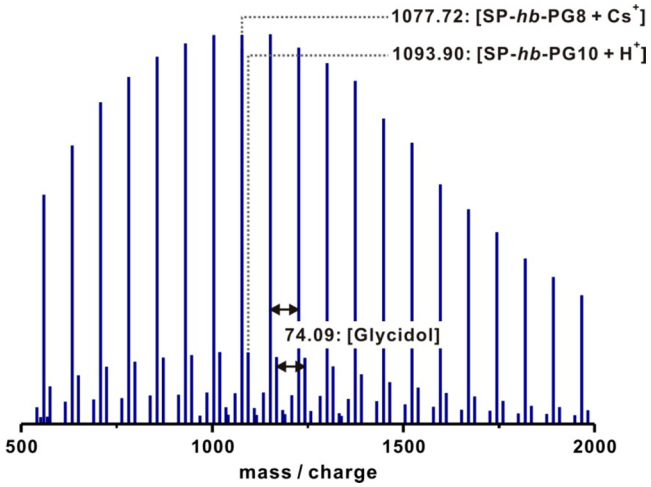

Figure 1. MALDI-ToF spectrum of SP-*hb*-PG_{15} (Entry 1 of Table 1), confirming each segment of SP-*hb*-PG.

shown in Figure 1, the main molecular weight distribution at 1077.72 corresponds to the molecular weight of SP-*hb*-PG with cesium as a counterion (SP(352) + PG(74.09) × 8 + Cs^+(133)) and the other molecular weight subdistribution at 1093.90 corresponds to the molecular weight of SP-*hb*-PG with H^+ as a counterion (SP(352) + PG(74.09) × 10 + H^+(1)). In addition, the spacing between the main- and the subdistribution matches well with the molecular weight of the glycidol monomer, 74.09 g/mol, which indicates the successful polymerization of SP-*hb*-PG.

Micelle Formulation and Reversible Micelle System. As explained in the Experimental Section, the micelles were prepared from the amphiphilic SP-*hb*-PG_{29} polymers by initial dissolution in DMF followed by the slow addition of excess amounts of DI water with subsequent dialysis. After preparation of the micelles, their morphology was investigated using transmission electron microscopy (TEM) and atomic force microscopy (AFM; Figure 2). Based on the TEM and AFM images, the micelles possessed a spherical structure with a relatively narrow size distribution. The diameter of the micelles based on each measurement was similar, with values of 31.3 ± 8.1 nm (TEM) and 38.2 ± 9.4 nm (AFM), respectively.

The UV-responsive nature of the SP-*hb*-PG polymers was evaluated by means of UV/vis spectroscopy, where isomerization of the SP segment was induced by irradiation. Under irradiation with UV light (365 nm) for 30 min, a new absorption band appeared at 550 nm, corresponding to the absorption of MC, which reflects the isomerization of SP to generate the MC form (see Supporting Information, Figure S3). The solution color also changed from colorless to light pink upon UV irradiation. In contrast, the new peak disappeared under illumination with visible light (620 nm), which suggests the isomerization of MC to the SP form in the SP-*hb*-PG polymer. Interestingly, we found that this reversible isomerization could be repeated several times without any changes in the spectrum of SP-*hb*-PG (see Supporting Information, Figure S3).

As a result of structural isomerization of neutral SP to zwitterionic MC, the amphiphilic SP-*hb*-PG is converted to the all-hydrophilic MC-*hb*-PG, which eventually drives the disassembly of the polymeric micelles, as illustrated in Scheme 1. This reversible micelle assembly and disassembly was monitored by using dynamic light scattering (DLS; Figure 3). The average diameter of the SP-*hb*-PG micelles measured by DLS was 33.2 ± 11.8 nm, which is similar to that determined from TEM and AFM measurement (Figure 2). Interestingly, the average diameter of the SP-*hb*-PG polymer decreased significantly to about 0.1 nm upon irradiation with UV light at 365 nm for 30 min, suggesting complete disassembly of the micelles into individual polymeric chains. This solution was again treated with visible light at 620 nm, at which point the average diameter returned to about 30 nm, similar to that of the initial micelles. The reversible nature of the micelle systems was confirmed from repeated DLS measurements. Light responsive deconstruction of micelle structures is important because after the delivery of a drug to a site using the micelles of SP-*hb*-PG, the structures can potentially disassemble into all-hydrophilic polymers of MC-*hb*-PG, which can be readily cleared and biodegraded.

Furthermore, we evaluated the potential of the SP-*hb*-PG polymer micelles in carrying a model hydrophobic therapeutic, pyrene. First, to estimate the amphiphilicity of SP-*hb*-PG, the critical micelle concentrations (CMCs) of all SP-*hb*-PG polymers were determined via an established CMC measurement method using pyrene.[30,31] A higher concentration of polymer solution induced greater encapsulation of pyrene, which resulted in a red-shift of the excitation band at 334 nm and an increase in the intensity of the excitation band (see Supporting Information, Figure S4). To measure the shift of the excitation band, the ratio of the fluorescence intensity at 339 and 332 nm (I_{339}/I_{332}) was plotted as a function of the concentration of SP-*hb*-PG, in which a clear crossover point was observed in the low concentration range of 10 to 20 mg/L, corresponding to the CMC value. As summarized in Table 1, the CMC values of all of the polymers show that increasing the mass of the hydrophilic segment of SP-*hb*-PG from 1500 to 3000 effectively increased the CMC values from 13 to 20 mg/L (Table 1). This observation can be attributed to the decreased hydrophobicity that efficiently reduced the segregation of the polymer blocks to accommodate the model hydrophobic therapeutics. This result is also consistent with our previous report.[26] Because a longer glycerol segment reduces the amphiphilicity of the SP-*hb*-PG polymer, it is reasonable that the micelle formation of the amphiphilic polymer is generated at a higher concentration.

Independent of the DLS measurement, the reversible nature of the micelle assembly and disassembly with pyrene can be characterized. As shown in Figure 4, the intensity of the

dx.doi.org/10.1021/bm401670t | *Biomacromolecules* 2014, 15, 628−634

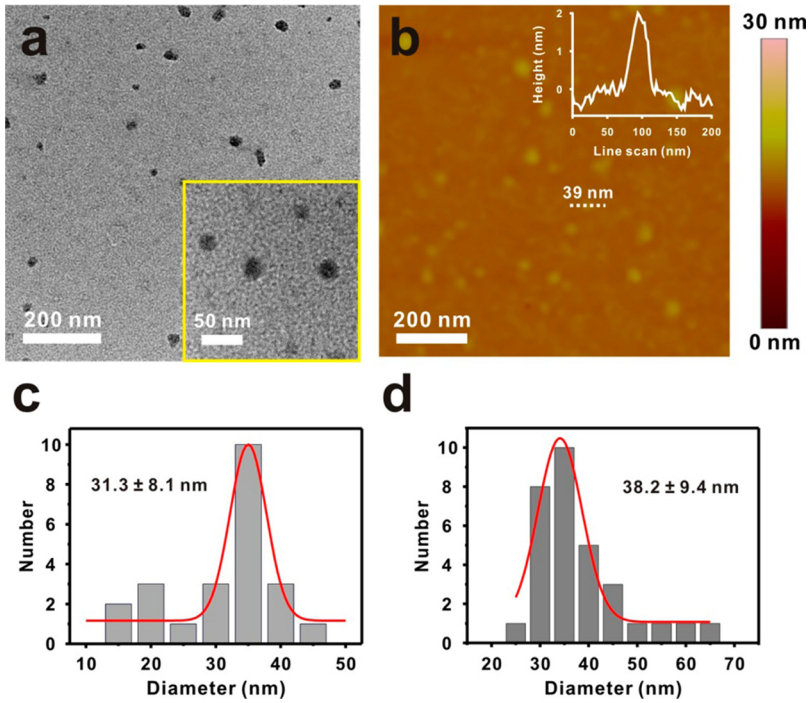

Figure 2. (a) TEM and (b) height-mode AFM images of SP-*hb*-PG_{29} micelles. (c, d) Corresponding size distributions determined by TEM and AFM showing an average diameter of 31.3 and 38.2 nm, respectively. Inset in (a) shows spherical morphology of micelles.

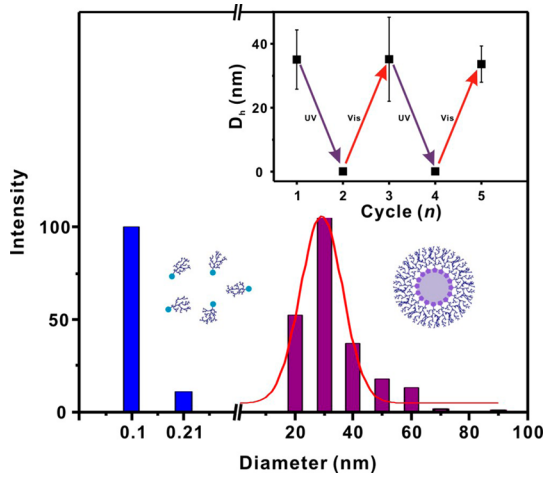

Figure 3. Size distribution of polymeric micelle (under irradiation with 620 nm visible light, purple column) and polymer chain (under 365 nm UV light, blue column) of SP-*hb*-PG_{29} determined by DLS. Inset graph shows the diameter of SP-*hb*-PG_{29} polymeric micelles and polymeric chain under repetitive irradiation cycles using UV and visible light.

fluorescence excitation band decreases depending on the UV irradiation time; this change is saturated after about 20 min with a slight blue-shift, indicating the release of pyrene from the micelle core. Interestingly, the plot of I_{339}/I_{332} with respect to the UV irradiation time shows a trend similar to the CMC experiment, which suggests degradation of the micelles. Moreover, the intensity of the fluorescence excitation spectra increases upon visible light irradiation. This observation is attributed to the re-encapsulation of released pyrene back into the micelle core, leading to the enhanced fluorescence band of the incorporated pyrene. However, this increase of the excitation intensity is terminated at 120 min and the recovered intensity is only about 40% of the initial intensity. This result implies that some portion of the released pyrene is not completely reloaded into the SP-*hb*-PG micelle core (Figure 4a). It should be noted that 254 nm UV irradiation was employed in this case because of the enhanced release kinetics of pyrene from the micelle core compared to 365 nm irradiation (see Supporting Information, Figure S5). On the other hand, it should be also considered that the irradiation at 254 nm may induce the cell toxicity during the micelle disassembly (about 88.2% cell viability for HeLa cells after 30 min irradiation). We found that the cell viability varied depending on the wavelength and duration of the UV irradiation as similarly observed in other report (see Supporting Information, Figure S6).[32] Therefore, the current UV irradiation approach needs a better control to enhance the kinetics of demicellization while minimizing the cell toxicity induced by the irradiation, which will be the subject of our ongoing research.

Finally, we evaluated the cytotoxicity of SP-*hb*-PGs to investigate their potential as a drug delivery carrier. The in vitro cytotoxicity of SP-*hb*-PGs was assessed by MTT assay using WI-38 cells and HeLa cells as respective models of normal and cancer cells (Figure 5). As a representative example, the viability of both cells after treating the SP-*hb*-PG_{36} micelle solution with varying concentrations was nearly 100%, even at a high concentration of 1000 μg/mL. These results indicate that the SP-*hb*-PGs are highly biocompatible and nontoxic to both cell lines. We cannot exclude the fact that the uptake efficiency of the SP-*hb*-PG micelles is relatively low; however, our previous report of doxorubicin-conjugated polyglycerol micelles are readily internalized into the HeLa cells as proved by the confocal fluorescence microscopy.[25] In other studies, a good cellular uptake of rhodamine-labeled hyperbranched PGs toward various types of cancer cell lines was demonstrated.[33,34] Taken together these evidences in the literature, we postulate

dx.doi.org/10.1021/bm401670t | *Biomacromolecules* 2014, 15, 628−634

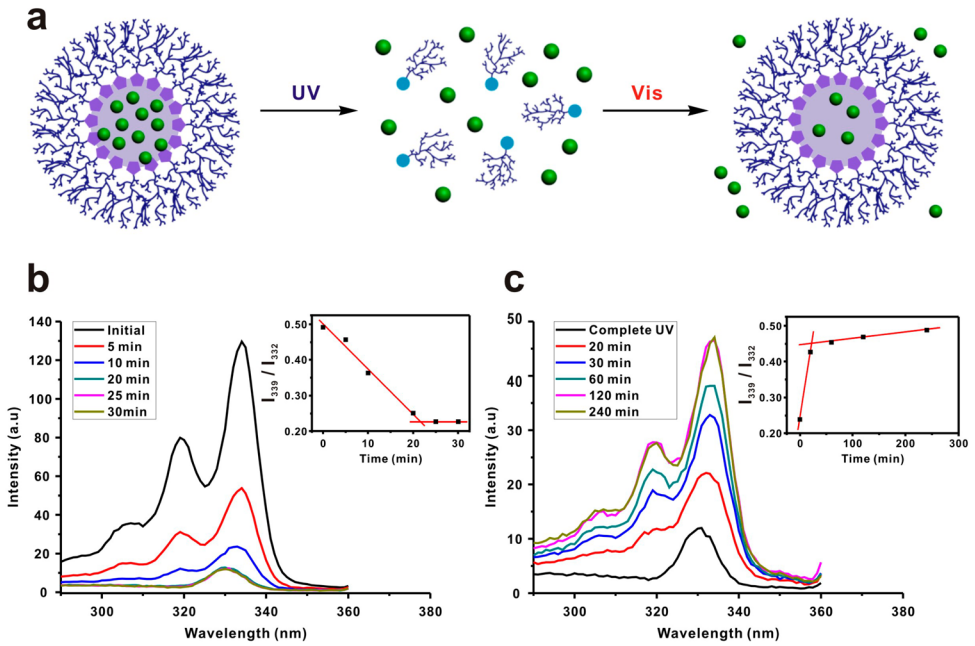

Figure 4. (a) Illustration of pyrene release upon 254 nm UV irradiation and re-encapsulation upon 620 nm visible irradiation of SP-*hb*-PG micelles. (b) Changes in excitation spectrum of pyrene encapsulated by SP-*hb*-PG_{29} micelle under 254 nm UV irradiation and (c) 620 nm visible irradiation. Inset shows the plot of I_{339}/I_{332} vs the exposure time to UV and visible light, respectively.

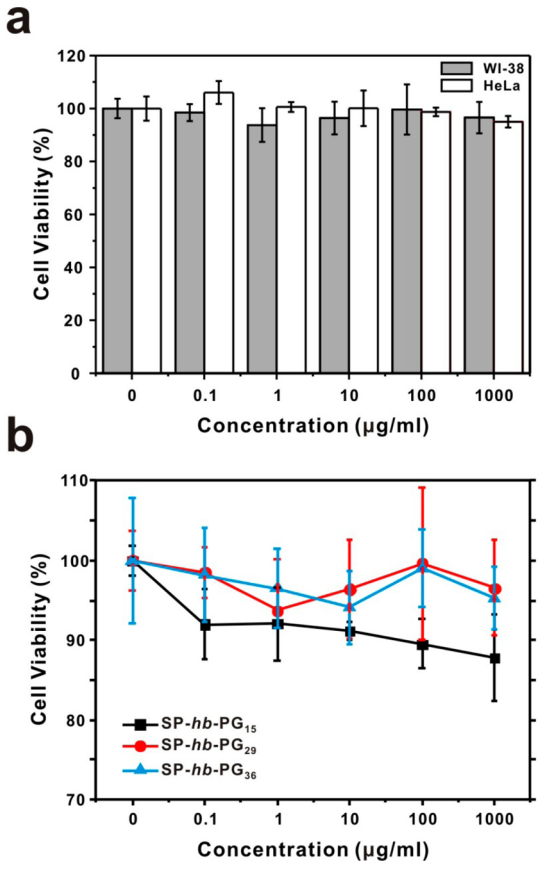

Figure 5. (a) Plot of cell viability of SP-*hb*-PG_{36} micelles determined by MTT assay; (b) WI-38 (normal cell) viability of all SP-*hb*-PG_n polymers.

that the similarly structured SP-*hb*-PG would undergo a similar process to be internalized into the HeLa cells without exhibiting significant cytotoxicity.

In addition, comparison of the toxicity of SP-*hb*-PGs toward normal WI-38 cells shows that an increase of the glycerol fraction is accompanied by slightly lowered cytotoxicity (Figure 5b). It is reasonable that SP-*hb*-PG of higher molecular weight exhibits greater biocompatibility due to the presence of a large fraction of highly biocompatible PG.

CONCLUSION

A novel light-responsive micelle system was developed using SP-*hb*-PG. Because of its considerable amphiphilicity, SP-*hb*-PG formed self-assembled polymeric micelles in aqueous medium. However, upon exposure to UV irradiation, the initially hydrophobic SP isomerized to zwitterionic MC, leading to the disassembly of the micelle structures. This structural change of the micelles was reversible upon exposure to visible light irradiation. The potential of the SP-*hb*-PG micelle for use as a smart drug delivery system was investigated using pyrene as a model hydrophobic therapeutic. The study suggested successful loading and release of pyrene upon external UV irradiation. In addition, the in vitro cytotoxicity of the SP-*hb*-PG polymers was evaluated using WI-38 and HeLa cells, demonstrating the excellent biocompatibility and nontoxicity of the SP-*hb*-PG micelles. We anticipate that this light-responsive smart drug delivery system will provide a new means to sophisticated delivery of active therapeutics in a time-specific and stimuli-specific manner.

ASSOCIATED CONTENT

Supporting Information

Additional ^{1}H and ^{13}C NMR spectra, UV/vis spectra, excitation spectra, and MTT assay. This material is available free of charge via the Internet at http://pubs.acs.org.

AUTHOR INFORMATION

Corresponding Author

*E-mail: bskim19@unist.ac.kr.

Notes

The authors declare no competing financial interest.

■ ACKNOWLEDGMENTS

This work was supported by the National Research Foundation of Korea (NRF) grant funded by the Korean government (No. 2010-0028684).

■ REFERENCES

(1) Wang, X.; Li, J.; Wang, Y.; Cho, K. J.; Kim, G.; Gjyrezi, A.; Koenig, L.; Giannakakou, P.; Shin, H. J. C.; Tighiouart, M.; Nie, S.; Chen, Z.; Shin, D. M. *ACS Nano* **2009**, *3*, 3165−3174.
(2) Phillips, M. A.; Gran, M. L.; Peppas, N. A. *Nano Today* **2010**, *5*, 143−159.
(3) Moghimi, S. M.; Hunter, A. C.; Murray, J. C. *FASEB J.* **2005**, *19*, 311−330.
(4) Ganta, S.; Devalapally, H.; Shahiwala, A.; Amiji, M. *J. Controlled Release* **2008**, *126*, 187−204.
(5) Peer, D.; Karp, J. M.; Hong, S.; Farokhzad, O. C.; Margalit, R.; Langer, R. *Nat. Nanotechnol.* **2007**, *2*, 751−760.
(6) Kim, B.-S.; Park, S. W.; Hammond, P. T. *ACS Nano* **2008**, *2*, 386−392.
(7) Kim, B.-S.; Smith, R. e. C.; Poon, Z.; Hammond, P. T. *Langmuir* **2009**, *25*, 14086−14092.
(8) Kataoka, K.; Harada, A.; Nagasaki, Y. *Adv. Drug Delivery Rev.* **2012**, *64*, 37−48.
(9) Rapoport, N. *Prog. Polym. Sci.* **2007**, *32*, 962−990.
(10) Fleige, E.; Quadir, M. A.; Haag, R. *Adv. Drug Delivery Rev.* **2012**, *64*, 866−884.
(11) Meng, F.; Zhong, Z.; Feijen, J. *Biomacromolecules* **2009**, *10*, 197−209.
(12) Han, D.; Tong, X.; Zhao, Y. *Macromolecules* **2011**, *44*, 437−439.
(13) Jiang, J.; Qi, B.; Lepage, M.; Zhao, Y. *Macromolecules* **2007**, *40*, 790−792.
(14) Wang, G.; Tong, X.; Zhao, Y. *Macromolecules* **2004**, *37*, 8911−8917.
(15) Cabane, E.; Malinova, V.; Meier, W. *Macromol. Chem. Phys.* **2010**, *211*, 1847−1856.
(16) Kainthan, R. K.; Janzen, J.; Levin, E.; Devine, D. V.; Brooks, D. E. *Biomacromolecules* **2006**, *7*, 703−709.
(17) Sunder, A.; Hanselmann, R.; Frey, H.; Mülhaupt, R. *Macromolecules* **1999**, *32*, 4240−4246.
(18) Schull, C.; Gieshoff, T.; Frey, H. *Polym. Chem.* **2013**, *4*, 4730−4736.
(19) Siegers, C.; Biesalski, M.; Haag, R. *Chem.—Eur. J.* **2004**, *10*, 2831−2838.
(20) Wilms, D.; Stiriba, S.-E.; Frey, H. *Acc. Chem. Res.* **2009**, *43*, 129−141.
(21) Wurm, F.; Nieberle, J.; Frey, H. *Macromolecules* **2008**, *41*, 1909−1911.
(22) Wilms, V. S.; Bauer, H.; Tonhauser, C.; Schilmann, A.-M.; Müller, M.-C.; Tremel, W.; Frey, H. *Biomacromolecules* **2012**, *14*, 193−199.
(23) Nuhn, L.; Schüll, C.; Frey, H.; Zentel, R. *Macromolecules* **2013**, *46*, 2892−2904.
(24) Kainthan, R. K.; Janzen, J.; Kizhakkedathu, J. N.; Devine, D. V.; Brooks, D. E. *Biomaterials* **2008**, *29*, 1693−1704.
(25) Lee, S.; Saito, K.; Lee, H.-R.; Lee, M. J.; Shibasaki, Y.; Oishi, Y.; Kim, B.-S. *Biomacromolecules* **2012**, *13*, 1190−1196.
(26) Oikawa, Y.; Lee, S.; Kim, D. H.; Kang, D. H.; Kim, B.-S.; Saito, K.; Sasaki, S.; Oishi, Y.; Shibasaki, Y. *Biomacromolecules* **2013**, *14*, 2171−2178.
(27) Berkovic, G.; Krongauz, V.; Weiss, V. *Chem. Rev.* **2000**, *100*, 1741−1754.
(28) Lee, H. i.; Wu, W.; Oh, J. K.; Mueller, L.; Sherwood, G.; Peteanu, L.; Kowalewski, T.; Matyjaszewski, K. *Angew. Chem., Int. Ed.* **2007**, *46*, 2453−2457.
(29) Raymo, F. M.; Giordani, S. *J. Am. Chem. Soc.* **2001**, *123*, 4651−4652.
(30) Wilhelm, M.; Zhao, C. L.; Wang, Y.; Xu, R.; Winnik, M. A.; Mura, J. L.; Riess, G.; Croucher, M. D. *Macromolecules* **1991**, *24*, 1033−1040.
(31) Wolf, F. K.; Hofmann, A. M.; Frey, H. *Macromolecules* **2010**, *43*, 3314−3324.
(32) Masuma, R.; Kashima, S.; Kurasaki, M.; Okuno, T. *J. Photochem. Photobiol., B* **2013**, *125*, 202−208.
(33) Mugabe, C.; Matsui, Y.; So, A. I.; Gleave, M. E.; Heller, M.; Zeisser-Labouèbe, M.; Heller, L.; Chafeeva, I.; Brooks, D. E.; Burt, H. M. *Biomacromolecules* **2011**, *12*, 949−960.
(34) Hu, M.; Chen, M.; Li, G.; Pang, Y.; Wang, D.; Wu, J.; Qiu, F.; Zhu, X.; Sun, J. *Biomacromolecules* **2012**, *13*, 3552−3561.